amplitude of the superlattice reflections of $Au_{77}Mg_{23}$ and $Au_{77}Cd_{23}$ which have a two-dimensional long-period antiphase structure based on the h.c.p. structure (Shindo, Hiraga, Hirabayashi, Terasaki & Watanabe, 1983). It was noticed that the contrast of the high-resolution images of these alloys changes sensitively with the crystal thickness.

In deriving the equation for the dynamical factor, we neglected double-weak scattering (Gjönnes, 1965; Spence, 1978) on the basis of condition (6), and assumed either the weak-phase-object approximation (3) or the similar approximation of higher order (23). These approximations can be more appropriately applied to alloys of which the constituent atoms have similar atomic scattering factors. We also note that the approximation holds to greater thickness for electron microscopy with higher accelerating voltages, because the interaction constant becomes smaller. In the limiting case, when a thin film of ordered alloy composed of elements with similar atomic numbers is examined with a high-voltage electron microscope, the dynamical factor tends to take a constant value for the superlattice reflections which contribute to the high-resolution images; so kinematical interpretation in HREM may be possible. It should be noted that the above argument can be applied to not only such simple ordered structures as discussed here but also complicated ones such as two-dimensional long-period antiphase structures which satisfy the conditions (6) and (7). This is because the dynamical factor does not directly depend on the ordered atomic arrangements.

The authors wish to thank Dr K. Hiraga for invaluable discussions. They also thank Dr T. B. Williams for useful comments on the manuscript.

**References**


BRODDIN, D., VAN TENDELOO, G., VAN LANDUYT, J., AMELINCKX, S., PORTIER, R., GUYMONT, M. & LOISEAU, A. (1986). *Philos. Mag.* **A54**, 395-419.

COWLEY, J. M. (1981). *Diffraction Physics.* 2nd revised ed. Amsterdam: North-Holland.

COWLEY, J. M. & FIELDS, P. M. (1979). *Acta Cryst.* **A35**, 28-37.

COWLEY, J. M. & MOODIE, A. F. (1957). *Acta Cryst.* **10**, 609-619.

COWLEY, J. M. & MURRAY, R. J. (1968). *Acta Cryst.* **A24**, 329-336.

COWLEY, J. M. & POGANY, A. P. (1968). *Acta Cryst.* **A24**, 109-116.

FISHER, P. M. J. (1965). *Proc. Int. Conf. Electron Diffraction and Crystal Defects*, paper IH-4. Melbourne: Australian Academy of Science.

FUJITA, F. E. & HIRABAYASHI, M. (1986). *Microscopic Methods in Metals*, edited by U. GONSER. Berlin: Springer-Verlag.

GJÖNNES, J. K. (1965). *Proc. Int. Conf. Electron Diffraction and Crystal Defects*, paper IH-2. Melbourne: Australian Academy of Science.

HIRAGA, K., HIRABAYASHI, M., TERASAKI, O. & WATANABE, D. (1982). *Acta Cryst.* **A38**, 269-274.

HIRAGA, K., SHINDO, D., HIRABAYASHI, M., TERASAKI, O. & WATANABE, D. (1980). *Acta Cryst.* **B36**, 2550-2554.

LEE, K. H., HIRAGA, K., SHINDO, D. & HIRABAYASHI, M. (1988). *Acta Metall.* **36**, 641-649.

SHINDO, D. (1982). *Acta Cryst.* **A38**, 310-317.

SHINDO, D., HIRAGA, K. & HIRABAYASHI, M. (1984). *Sci. Rep. Res. Inst. Tohoko Univ. Ser. A*, **32**, 32-45.

SHINDO, D., HIRAGA, K., HIRABAYASHI, M., TERASAKI, O. & WATANABE, D. (1983). *J. Appl. Cryst.* **16**, 233-238.

SPENCE, J. C. H. (1978). *Acta Cryst.* **A34**, 112-116.

SPENCE, J. C. H. (1981). *Experimental High-Resolution Electron Microscopy.* Oxford: Clarendon Press.

TAKEDA, S., KULIK, J., DE FONTAINE, D. & TANNER, L. E. (1986). *Proc. 11th Int. Congr. on Electron Microscopy*, edited by T. IMURA, S. MARUSE & T. SUZUKI, pp. 957-958. Kyoto: Japanese Society of Electron Microscopy.

TANAKA, N. & COWLEY, J. M. (1987) *Acta Cryst.* **A43**, 337-346.

TERASAKI, O., MIKATA, Y., WATANABE, D., HIRAGA, K., SHINDO, D. & HIRABAYASHI, M. (1982). *J. Appl. Cryst.* **15**, 65-71.

VAN DYCK, D., VAN TENDELOO, G. & AMELINCKX, S. (1982). *Ultramicroscopy*, **10**, 263-280.

VAN TENDELOO, G. & AMELINCKX, S. (1985). *Acta Cryst.* **B41**, 281-292.


*Acta Cryst.* (1988). **A44**, 960-965

# A Top–Bottom Contrast Effect in Dark-Field Images Arising from *N*-Beam Dynamic Refraction

BY F. FUJIMOTO

*College of General Education, University of Tokyo, Komaba, Megura, Tokyo* 153, *Japan*

AND P. GOODMAN

*School of Physics, University of Melbourne, Parkville, Australia* 3052

(*Received* 7 *December* 1987; *accepted* 22 *June* 1988)

**Abstract**

The refraction effect associated with an off-Bragg diffracted beam in high-energy transmission electron diffraction is analysed. It is found that the wave vectors of Bloch-wave components of a beam associated with a finite excitation error are significantly shortened or lengthened as a consequence of dynamic scattering, with the direction of change being determined by the sign of the excitation error. By

0108-7673/88/060960-06$03.00 

consideration of the dark-field image formed from the off-Bragg reflection and its associated refractive fine structure it is shown that a top-bottom effect exists, which can be demonstrated by comparing images of the same field for positive and negative excitation errors. This is discussed in two dimensions for a crystal of triangular cross section and one horizontal face, in the two orientations of apex up and apex down, with numerical and graphical evaluations from linear three-beam diffraction.

## 1. Introduction

When a parallel beam of electrons passes through a wedge-shaped crystal the diffraction spots on the back-focal plane are split, allowing observation of the separate Bloch-wave components in intensity, in contrast to the parallel-sided crystal case where these are all recombined at the exit crystal face. This effect was explained by Kato (1952) in the two-beam approximation and by one of the present authors (Fujimoto, 1965) by incorporating a crystal shape function in the $N$-beam dynamic equations.

The real-space consequence of the above phenomenon is the *Pendellösung* fringe of electron microscopy. It is somewhat surprising to find that although these fringes have been closely studied and utilized for two decades for the case of a single-wedge (*i.e.* semi-infinite) crystal, the case of a multi-wedge or finite polyhedral crystal has never been considered in detail. In particular, for an image away from the Gaussian plane, the relative phases of transmitted waves from adjacent facets either side of a surface step is of importance. This importance was made clear by the results of Goodman & McLean (1976), who were, however, unable to give a reasonable explanation for their results. In the present paper we show that the refraction effect in many-beam diffraction is sufficient to explain the top-bottom effect observed by these authors.

## 2. Many-beam theory

According to the $N$-beam Bloch-wave dynamical theory (*e.g.* Fujimoto, 1959, 1960), the wave-vector amplitude for the $g$ reflection in a crystal belonging to the $i$th Bloch-wave field is given by

$$|\mathbf{k}_g^i| = |\mathbf{k}_0 - \zeta_g + \xi^i|, \tag{1}$$

where $\mathbf{k}_0$ is the incident wave vector in the crystal, $\zeta_g$ the excitation error for the $g$ reflection and $\xi^i$ the *Anpassung* obtained by solving the secular equation

$$\begin{vmatrix} \cdots & \cdots & \cdots & \cdots & \cdots & \cdots & \cdots \\ \cdots & 2k_0(-\zeta_g+\xi) & \cdots & v_g & \cdots & v_{h+g} & \cdots \\ \cdots & v_{-g} & \cdots & 2k_0\xi & \cdots & v_h & \cdots \\ \cdots & v_{-(h+g)} & \cdots & v_{-h} & \cdots & 2k_0(-\zeta_h+\xi) & \cdots \\ \cdots & \cdots & \cdots & \cdots & \cdots & \cdots & \cdots \end{vmatrix} = 0. \tag{2}$$

$v_h$ is a Fourier component of the crystal potential $V(r)$ multiplied by $(-2m/h^2)$, so that

$$-\frac{2m}{h^2}V(r) = -\frac{2m}{h^2}\sum_h V_h \exp(i\mathbf{b}_h\mathbf{r}) = \sum_h v_h \exp(i\mathbf{b}_h\mathbf{r}), \tag{3}$$

$\mathbf{b}_h$ being the reciprocal vector multiplied by $2\pi$ for the $h$ reflection. Using the convention whereby the capitals $\mathbf{K}_0$, $\mathbf{K}_0^i$, $\mathbf{K}_g^i$ *etc.* denote waves outside the crystal and all have the same magnitude, while the lower-case designations $\mathbf{k}_0^i$, $\mathbf{k}_h^i = \mathbf{k}_0 + \mathbf{b}_h$ *etc.* refer to waves inside the crystal, we proceed to derive relationships between various sets. Thus the magnitude of $\mathbf{k}_0$ is given by

$$|\mathbf{k}_0| = [(2m/h^2)(E_0 + V_0)]^{1/2} \simeq |\mathbf{K}_0|(1 + \tfrac{1}{2}V_0/E_0) \tag{4}$$

where $E_0$ and $K_0$ are the energy of the incident electron and its wave vector in vacuum, respectively. The magnitude and direction of $\mathbf{k}_h^i$ are determined by the boundary condition at the entrance surface, *i.e.* the tangential components of $\mathbf{K}_0$, and the $\mathbf{k}_h^i$'s are equal, as seen in Fig. 1, *i.e.*

$$\left.\begin{aligned} |\mathbf{K}_0|_t &= |\mathbf{k}_0^{i_1,i_2,\cdots}|_t \\ \text{and} \quad |\mathbf{K}_h^{i_1,i_2,\cdots}|_t &= |\mathbf{k}_0^{i_1,i_2,\cdots}|_t + \mathbf{b}_h. \end{aligned}\right\} \tag{5}$$

The wave function in the crystal is given by

$$\Psi(\mathbf{r}) = \sum_i \sum_h \psi_0^{i*}\psi_h^i \exp(i\mathbf{k}_h^i\mathbf{r}) \tag{6}$$

where $\psi_h^i$ is the normalized wave amplitude given by

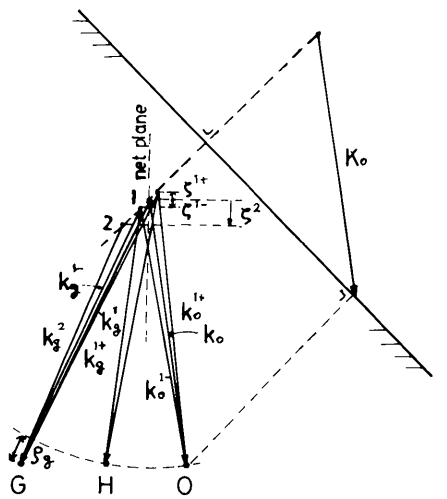


Fig. 1. Three-beam diagram showing the relationships between the wave vectors, the excitation error and the *Anpassung* values.

solving the equations

$$\begin{aligned}
&\ldots+2k_0(-\zeta_g+\xi^i)\psi_g^i+\ldots+v_g\psi_0^i\\
&\qquad+\ldots+v_{h+g}\psi_h^i+\ldots=0\\
&\ldots+v_{-g}\psi_g^i+\ldots+2k_0\xi^i\psi_0^i\\
&\qquad+\ldots+v_h\psi_h^i+\ldots=0\\
&\ldots+v_{-(h+g)}\psi_g^i+\ldots+v_{-h}\psi_0^i\\
&\qquad+\ldots+2k_0(-\zeta_h+\xi^i)\psi_h^i+\ldots=0,
\end{aligned}\tag{7}$$

with

$$\sum_h|\psi_h^i|^2=1.$$

The wave emitted from the exit surface is composed of various partial waves, as

$$\Psi_e(\mathbf{r})=\sum_i\sum_h\psi_0^{i*}\psi_h^i\exp(i\delta^i)\exp(i\mathbf{K}_h^i\mathbf{r})\tag{8}$$

where the $\mathbf{K}_h^i$'s have the same magnitude as $\mathbf{K}_0$ and are subject to the same boundary conditions at the exit surface as in (5). $\delta_h^i$ is the phase shift due to the different magnitude of each wave vector in the crystal and is given by

$$\delta_h^i=(-\zeta_h+\xi^i)t_h^i,\tag{9}$$

$t_h^i$ being the path length of the wave $\mathbf{k}_h^i$ in the crystal, and $t_h^i=t\cos\theta_h^i$ for a crystal of thickness $t$. Because of this phase shift the intensity of the $h$ reflection changes with $t$ and is expressed by a sum of sinusoidal functions with various periods $T_{ij}$ as

$$T_{ij}=\pi/|\xi^i-\xi^j|,\tag{10}$$

though the sum, $\sum_h I_h$, of the diffracted transmitted intensities at the exit surface is unity. This phenomenon is the *Pendellösung*.

If the entrance and exit surfaces are not parallel, the directions of the wave vectors $\mathbf{k}_h^i$ for the $h$ reflection vary with $i$. This phenomenon is known as multiple refraction.

### 3. The off-Bragg reflection and its wave vector

For the remainder of this paper we will give a qualitative description of the top-bottom effect associated with off-Bragg reflections. For this purpose it is sufficient to consider all inner reflections concerned as either near-Bragg ($\zeta_h\simeq0$) or off-Bragg ($\zeta_g\ll0$ or $\gg0$), for which cases either the *Anpassung* $\xi^i$, or excitation error $\zeta_g$ dominate (1), and for these two classes we will use the indices $h$ and $g$, respectively. The top-bottom effect is most readily derived from the linear systematic three-beam case for $O$, $G$ and $H$ beams illustrated in Fig. 1. The most important wave fields for the satisfied $h$ reflection are those with $|\mathbf{k}_0^i|\simeq|\mathbf{k}_h^i|\simeq\mathbf{K}_0|$, *i.e.* approximately those given by the two-beam theory. Although in the general case there will be more than two wave fields, since we are here considering the simplest possible examples where there are only two important wave fields associated with the reflection of zero or near-zero excitation error, we designate the wave vectors as $\mathbf{k}_h^+$ and $\mathbf{k}_h^-$, corresponding to the *Anpassung* values

$$\xi^{\pm}=\pm|v_h/2k_0|.\tag{11}$$

The important wave fields for the $g$ reflection are similarly those for which $|\mathbf{k}_g^i|\simeq|\mathbf{K}_0|$, and their number can be two or more depending upon the precise diffraction conditions. However, the differences among the $\xi^i$'s corresponding to these wave vectors, as well as their absolute values, are generally small compared with the excitation error $\zeta_g$ where this has a significant value (*i.e.* relates to an off-Bragg reflection).

Now we wish to estimate the magnitude of the relevant parameters, for the two classes of reflections given by $\zeta_g=0$, and $\zeta_g\gg0$ or $\zeta_g\ll0$. In the case of an MgO crystal at 100 kV, $V_0=15$, $V_{220}=5$ and $V_{440}=1{\cdot}5$ eV, and the wavelength and lattice constant are $\lambda=0{\cdot}037$ and $a=4{\cdot}2$ Å respectively. The lattice spacing $d_{220}$ is 1·5 Å. Then we obtain the refraction relationships between $\mathbf{K}_0$, $\mathbf{k}_0$ and $\mathbf{k}_h$ as

$$|\mathbf{k}_0|=|\mathbf{K}_0|(1+V_0/E_0)^{1/2}=|\mathbf{K}_0|(1+7{\cdot}5\times10^{-5});$$

$$|\mathbf{k}_{220}|=|\mathbf{k}_0|(1\pm V_{220}/E_0)^{1/2}=|\mathbf{k}_0|(1\pm2{\cdot}5\times10^{-5}),$$

giving the diffracted crystal wave amplitudes for the exactly excited $h$ reflection shown in Fig. 1, with $h=220$.

$$|\mathbf{k}_{220}|^+=|\mathbf{K}_0|(1+1\times10^{-4});\ |\mathbf{k}_{220}|^-=|\mathbf{K}_0|(1+5\times10^{-5}).\tag{12}$$

For the off-Bragg $g$ reflection, the magnitude of the wave vectors depends on the sign of $\zeta_g$, *i.e.* upon whether the reciprocal-lattice point $G$ is located outside or inside the Ewald sphere. For simplicity we consider the orientations of Figs. 2(*a*) and (*b*) with (*a*) $h=220$ and $g=440$; $\zeta_g<0$; and (*b*) $h=440$ and $g=220$; $\zeta_g>0$.

When $\zeta_g\gg$, as for the Bloch wave 1, we can obtain estimates for the $|\mathbf{k}_g^i|$ amplitudes geometrically.

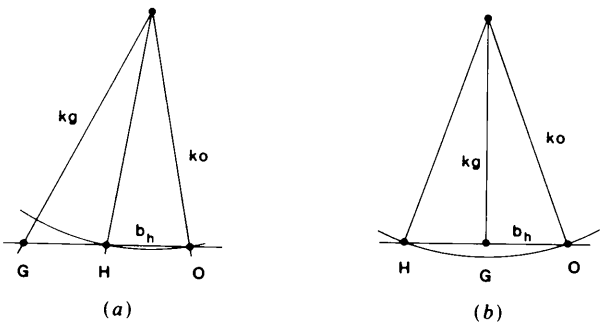


Fig. 2. The three-beam orientations for the conditions (*a*) and (*b*) of the text.

Hence: for ($a$),

$$k^1_{440} \simeq [(3b_n/2)^2 + (k_0 \cos\theta_n)^2]^{1/2}$$
$$= |\mathbf{k}_0|[1 + 2(b_h/k_0)^2]^{1/2}$$
$$= |\mathbf{k}_0|(1 + 6\times 10^{-4}) = |\mathbf{K}_0|(1 + 6{\cdot}8\times 10^{-4}) \quad (13)$$

and for ($b$),

$$|\mathbf{k}^1_{220}| \simeq [k_0^2 - b_h^2]^{1/2} = |\mathbf{k}_0|[1 - (b_h/k_0)^2]^{1/2}$$
$$= |\mathbf{k}_0|(1 - 3\times 10^{-4}) = |\mathbf{K}_0|(1 - 2{\cdot}3\times 10^{-4}). \quad (14)$$

These estimates show that $\mathbf{k}^1_{440}$ is significantly longer than $\mathbf{k}_0$ and $\mathbf{K}_0$ and $\mathbf{k}^1_{220}$ is shorter than $\mathbf{K}_0$. This indicates that the refraction effect of the off-Bragg reflections is not only larger than the simple two-beam case of (12), but that also an effect of negative refraction arises for $\zeta_g > 0$.

The above condition on refraction, for important components of a weakly excited reflection, can also be deduced for the many-beam diffraction condition. This can be seen when we make the simplifying assumption that all the inner reflections involved can be classed as either strongly excited or weakly excited, and we are using one of the latter, $G$, for dark-field imaging. In this case the scattering paths involving more than one weakly excited beam will be less important than the others, for which the effect of $\zeta_g$ will dominate, and lead to a top-bottom effect in a similar manner to that demonstrated here for only three beams.

## 4. The top–bottom effect in off-Bragg images

We consider four cases, illustrated in Figs. 3($a$) and ($b$), 4($a$) and ($b$). Fig. 3 shows the two cases for the apex-up geometry while Fig. 4 shows the reverse orientation. Then ($a$) and ($b$) have the meaning ($a$) $\zeta_g < 0$ and ($b$) $\zeta_g > 0$, as in Fig. 2. In all cases the $h$ reflection is satisfied ($\zeta_h = 0$). The direction of waves leaving the crystal is shown in the four cases. These results clearly show that the components of one of the two pairs of emitted plane waves for the $g$ reflection are either diverging or converging (indicated by arrows in the figures), while those for the other pair of waves are almost parallel, in each case. This is most clearly seen in the lowest set of drawings in each figure which show the Ewald construction for the existing waves. In each case the diverging, or converging, pair of wave vectors is indicated by a labelled ($D$ or $C$) bracket, indicating the relative sign of refraction from the left and right sides of the crystal.

For the satisfied $h$ reflection these effects are negligible. Not only is the influence of the weakly excited waves on the satisfied reflection very small, but also the components of the two pairs of emitted directions due to the $\mathbf{K}^1_h$ and $\mathbf{K}^2_h$ wave fields slightly converge

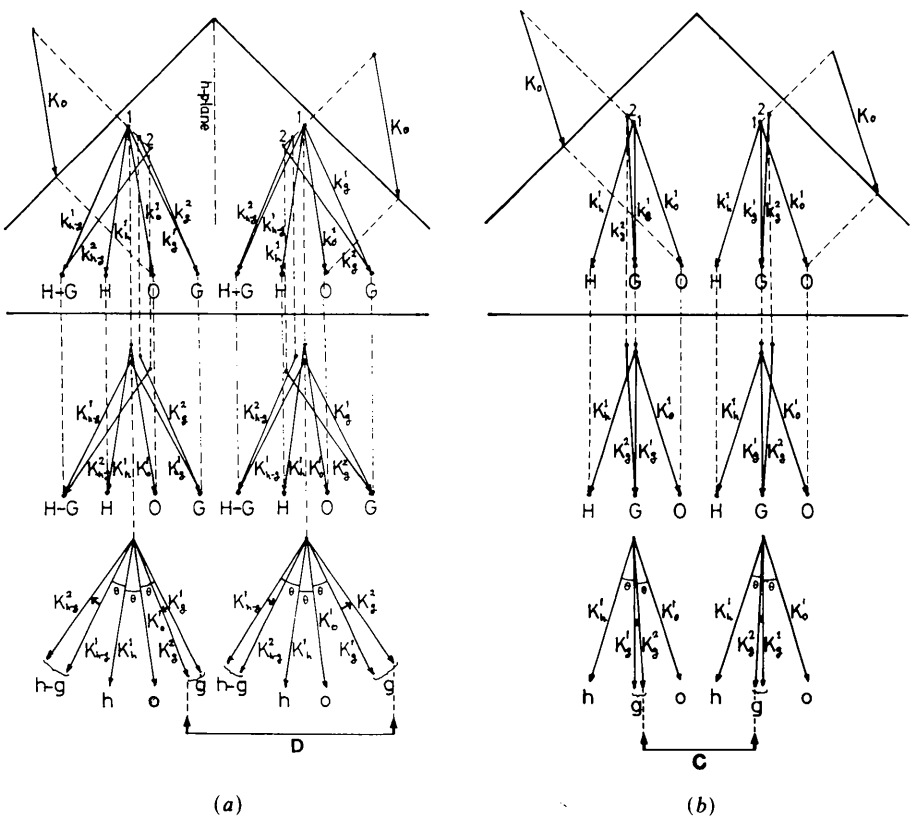


Fig. 3. Symmetrical three- and four-beam cases from the crystal geometry of 'apex-up'. ($a$) $\zeta_h = 0$; $\zeta_g = \zeta_{g-h} < 0$; ($b$) $\zeta_h = 0$; $\zeta_g > 0$. The three drawings, descending from top to bottom of the page, show successively the crystal waves, the vacuum exiting waves in dispersion-surface form, and the same waves in Ewald-sphere construction, respectively.

in both cases. For the incident beam $\mathbf{K}_0$ the situation is the same as for the satisfied reflection.

The resulting microscope contrast depends upon the focusing condition. For under-focus (Gaussian plane on the incident beam side), the dark-field $g$-beam images of the corner of the triangle are bright in Figs 3($a$) and 4($b$) and dark in 3($b$) and 4($a$). For over-focus, the contrast is reversed. This effect is emphasized with increasing magnitude of $\zeta_g$, and of defocus $\Delta f$.

These examples show the case of a triangular 'hill' on the surface. In the case of a triangular 'hollow' the contrast associated with the apex will be reversed.

By taking images for both $\Delta f < 0$ and $\Delta f > 0$ these two situations, *i.e.* the sign of the potential jump (more precisely the sign of the second differential of the projected potential) at the crystal apex may be determined, using either the bright-field- or dark-field-satisfied beam. This interpretation can be made using the projected potential approximation described by Lynch, Moodie & O'Keefe (1974).

For the dark-field images formed from the off-Bragg ($\zeta_g \neq 0$) beam a complete reversal of edge contrast also occurs with a change in the sign of defect of the focus. Therefore if the sign of $\varphi_p$ is pre-determined from another (zero-order or satisfied) beam, the allocation of apex to either top or bottom surface can be made from the off-Bragg image, knowing the sign of $\zeta_g$, from the above-described refraction effects, and in complete accord with the observations of Goodman & McLean (1976).

If an etch pit is very small, the contrast of its image is more complicated, but it *may* be observed as split lines or spots similar to those recently observed (Goodman & Warble, 1987) as a consequence of dynamic refraction. However, it may be difficult to distinguish small etch pits from top and bottom surfaces.

A top–bottom effect has been observed in the case of a grain boundary by Nonoyama, Nakai & Kamiya (1973). This effect was explained in terms of the difference between the absorption coefficients for off-Bragg and on-Bragg reflections. The present top–bottom effect is caused by a completely different phenomenon.

One of the authors (FF) sincerely thanks Professor L. T. Chadderton who gave him an opportunity to stay at the Division of Chemical Physics, and financial support. In addition the authors wish to thank the referees for their constructive suggestions.

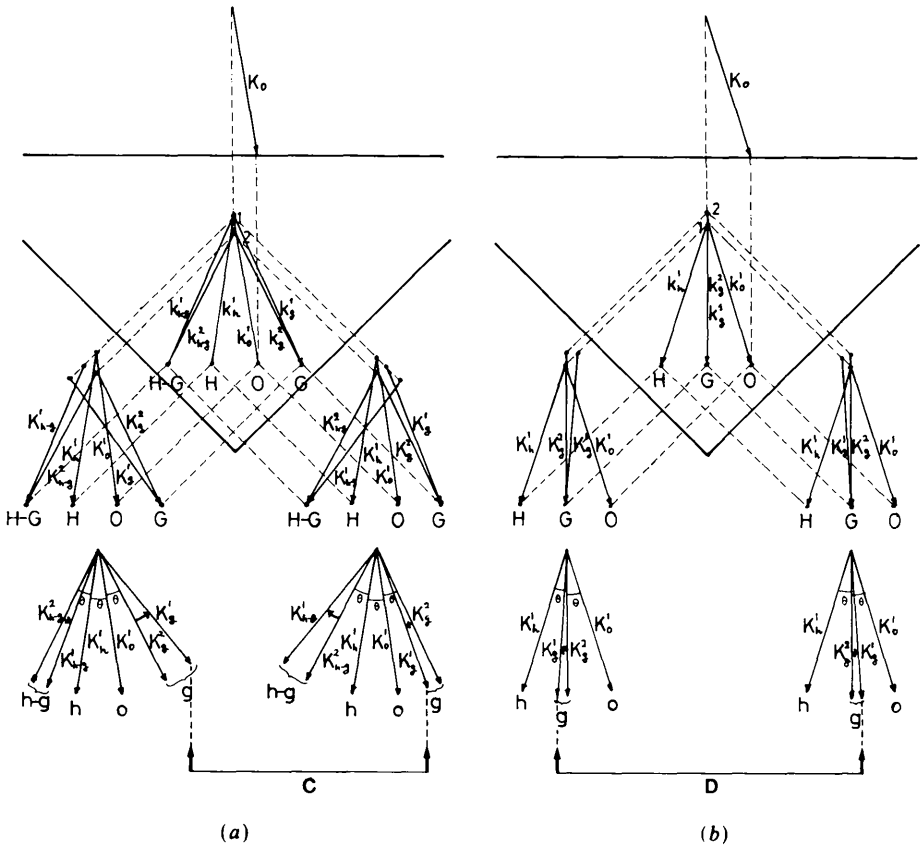


Fig. 4. Symmetrical three- and four-beam cases from the crystal geometry of 'apex-down'. ($a$) $\zeta_h = 0$; $\zeta_g = \zeta_{g-h} < 0$; ($b$) $\zeta_h = 0$; $\zeta_g > 0$. The wave depiction follows the same pattern as in Fig. 3.

**References**

FUJIMOTO, F. (1959). *J. Phys. Soc. Jpn*, **14**, 1558-1563.
FUJIMOTO, F. (1960). *J. Phys. Soc. Jpn*, **15**, 859-867.
FUJIMOTO, F. (1965). *Z. Naturforsch. Teil A*, **20**, 367-379.
GOODMAN, P. & MCLEAN, J. D. (1976). *Philos. Mag.* **34**, 861-876.
GOODMAN, P. & WARBLE, C. E. (1987). *Philos. Mag. B*, **56**, 15-30.
KATO, N. (1952). *J. Phys. Soc. Jpn*, **7**, 406-414.
LYNCH, D. F., MOODIE, A. F. & O'KEEFE, M. A. (1974). *Electron Microscopy* 1974. *Proc. 8th Int. Congress on Electron Microscopy, Canberra, Australia*, 1974. Australian Acad. Sci. Publ. pp. 222-223.
NONOYAMA, M., NAKAI, Y. & KAMIYA, Y. (1973). *J. Electron Microsc.* **22**, 231-241.

*Acta Cryst.* (1988). A**44**, 965-975

# The Development of *In Situ* High-Resolution Electron Microscopy

BY R. SINCLAIR, T. YAMASHITA, M. A. PARKER, K. B. KIM, K. HOLLOWAY AND A. F. SCHWARTZMAN

*Department of Materials Science and Engineering, Stanford University, Stanford, CA* 94305-2205, *USA*

(*Received* 4 *April* 1988; *accepted* 22 *June* 1988)

**Abstract**

Progress in introducing high-resolution electron microscopy at controlled elevated temperatures is described. Initial work involved the study of dynamic events in materials like cadmium telluride which can be heated to a sufficient degree by the imaging beam. However, for reproducible experiments the temperature must be carefully controlled and measured, and this involves a heating specimen holder. Results achieved recently this way on a variety of substances including CdTe, GaAs, Si, GaAs–Ti, GaAs–Ni, Si–Mo and Si–Ti, are reported. To derive information pertinent to bulk behavior both the manner of an *in situ* reaction and its kinetics should be compared with those for specimens prepared from macroscopic materials treated *ex situ*. For interface reactions in semiconductor materials it is found that events typical of the bulk can be recorded under high-resolution conditions in a large proportion of cases.

## Introduction

Following the first demonstration that the electron microscope is capable of resolving crystal lattices (Menter, 1956) and that images can be interpreted in terms of atomic postions (Cowley & Iijima, 1972), there have been increasing applications of high-resolution electron microscopy (HREM). The recording of dynamic events at atomic resolution is a natural extension of the technique since it presents the possibility that atomic behavior can be seen, and deduced, directly. Several examples are quite well known (Hashimoto, Takai, Yokota, Endo & Fukuta, 1980; Sinclair *et al.*, 1982; Eyring, Dutner, Goral & Holladay, 1985; Iijima & Ichihashi, 1986; Bovin, Wallenberg & Smith, 1986). One drawback of these early works has been that they rely either on the fortuitous occurrence of interesting events during the course of observation and recording, or on the imaging electron beam inducing changes in the sample. It has only recently been appreciated that heating holders have sufficient stability to allow image recording at elevated temperatures (Parker & Sinclair, 1985; Gibson, McDonald & Unterwald, 1985; Sinclair & Parker, 1986), so that natural thermally activated processes can also be studied. Of course this is an important development for fundamental investigations of reactions and transformations in solids. During the past year, we have applied this technique to a variety of interfacial annealing phenomena in semiconductor systems. This article describes some of this research and assesses its prospects for revealing atomic mechanisms in this important class of materials.

## Experimental considerations

As with all *in situ* transmission electron microscopy (TEM) experiments (*e.g.* Butler & Hale, 1981), images are obtained following normal procedures, with a special sample holder employed to manipulate the specimen temperature. For high-resolution imaging one critical parameter is the crystal orientation with respect to the incident beam, which generally requires use of a double-tilt specimen holder. Currently no such holder with heating capability is commercially available but we circumvented this problem by using cross-section specimens which are prepared with one low-index crystallographic direction easily identifiable macroscopically (Sinclair, Parker & Kim, 1987). In this case with a side-entry high-resolution TEM a single-tilt axis is sufficient for correct orientation.

Observations can be recorded continuously on videotape using an image pick-up system. The quality, especially with the new medium-voltage microscopes, is sufficiently good that atomic-level changes are easily seen without recourse to image processing. Micrographs for analysis or publication can be photographed from a video display either during playback

0108-7673/88/060965-11$03.00 